The Journal of Experimental Biology 209, 2535-2553
Published by The Company of Biologists 2006
doi:10.1242/jeb.02276

Storage and recovery of elastic potential energy powers ballistic prey capture in toads

A. Kristopher Lappin*, Jenna A. Monroy, Jason Q. Pilarski, Eric D. Zepnewski, David J. Pierotti and Kiisa C. Nishikawa*,†

Department of Biological Sciences, Northern Arizona University, Flagstaff, AZ 86011-5640, USA

*These authors contributed equally to this study

†Author for correspondence (e-mail: Kiisa.Nishikawa@nau.edu)

Accepted 18 April 2006

Summary

Ballistic tongue projection in toads is a remarkably fast and powerful movement. The goals of this study were to: (1) quantify *in vivo* power output and activity of the depressor mandibulae muscles that are responsible for ballistic mouth opening, which powers tongue projection; (2) quantify the elastic properties of the depressor mandibulae muscles and their series connective tissues using *in situ* muscle stimulation and force-lever studies; and (3) develop and test an elastic recoil model, based on the observed elastic properties of the depressor mandibulae muscles and series connective tissues, that accounts for displacement, velocity, acceleration and power output during ballistic mouth opening in toads. The results demonstrate that the depressor mandibulae muscles of toads are active for up to 250 ms prior to mouth opening. During this time, strains of up to 21.4% muscle resting length (*ML*) develop in the muscles and series connective tissues. At maximum isometric force, series connective tissues develop strains up to 14% *ML*, and the muscle itself develops strains up to 17.5% *ML*. When the mouth opens rapidly, the peak instantaneous power output of the depressor mandibulae muscles and series connective tissues can reach 9600 W kg^{-1}. The results suggest that: (1) elastic recoil of muscle itself can contribute significantly to the power of ballistic movements; (2) strain in series elastic elements of the depressor mandibulae muscle is too large to be borne entirely by the cross bridges and the actin–myosin filament lattice; and (3) central nervous control of ballistic tongue projection in toads likely requires the specification of relatively few parameters.

Key words: contractile properties, depressor mandibulae, elastic properties, elastic recoil model, load clamp, load dependence, parallel elastic component, series elastic component, power output, toad.

Introduction

Ballistic movements are those in which a body is propelled by an external force and continues in motion under its own inertia. Such movements typically accelerate from rest and are completed too quickly for feedback control. Hence, ballistic movements must be planned in advance (i.e. feed-forward control). For ballistic movements, such as jumping or throwing, power output likely sets the upper limit on maximum performance (Alexander, 1968; Askew and Marsh, 1998). During ballistic movements (e.g. jumping), it is generally believed that muscles store energy prior to movement by imposing a strain on stiffer structures, such as tendon or cuticle (Alexander and Bennet-Clark, 1977). The stored energy is recovered rapidly during the subsequent movement. Rapid recovery of stored energy provides higher power for ballistic movements than could be provided directly by the muscles because muscle contraction is much slower than elastic recoil of tendon or cuticle (Alexander, 2002). A classic example is the jump of the locust, in which the extensor tibiae muscle imposes a strain in its apodeme and the semilunar process of the cuticle prior to leg extension (Bennet-Clark, 1975; Burrows and Morris, 2001). Upon relaxation of the flexor tibiae, the apodeme and cuticle recoil elastically to increase power during jumping.

Ballistic tongue projection is a feeding mechanism in which the tongue is propelled from the oral cavity. Among vertebrates, only some anurans, some salamanders, and chameleons use ballistic tongue projection to capture prey (Nishikawa, 2000). Whereas power augmentation during jumping has been investigated in a wide variety of animals (e.g. Alexander, 1968; Lutz and Rome, 1994; Peplowski and Marsh, 1997; Aerts, 1998), fewer studies have addressed the question of power augmentation during ballistic tongue projection in chameleons (Wainwright and Bennett, 1992a; Wainwright and Bennett, 1992b; Meyers and Nishikawa, 2000; de Groot and van Leeuwen, 2004) and salamanders (Deban et al., 1997; Deban and Dicke, 1999). Yet, these ballistic tongue projection systems may provide ideal models for studying mechanisms of power augmentation because their anatomical

arrangements are relatively simple compared to those of the limbs (e.g. the jaws and hyolingual apparatus tend to possess fewer muscles and fewer joints than limbs). Also, in general, the origins and insertions of cranial and hyolingual muscles in vertebrates tend to be fleshy or possess very short aponeuroses and/or tendons compared to distal limb muscles. Thus, it is expected that cranial and hyolingual muscles would contribute more to the total strain and strain energy than muscles that possess longer tendons (Alexander, 1988).

Recent comparative studies have shown that, among anurans, toads (genus *Bufo*) appear to be particularly adapted for ballistic tongue projection (Nishikawa, 1999; Nishikawa, 2000). Forward-dynamic biomechanical models have shown that the paired depressor mandibulae muscles produce >90% of the force needed for ballistic tongue projection in anurans (Mallett et al., 2001). When these muscles open the mouth rapidly, momentum is transferred from the lower jaw to the tongue pad. Although previous studies have addressed the mechanism of tongue projection and have described the kinematics of ballistic jaw and tongue movements (Nishikawa and Gans, 1992; Nishikawa and Gans, 1996), no previous study has investigated mechanisms of power augmentation during ballistic mouth opening in toads.

The goals of the present study were to: (1) quantify the power output and patterns of activation of the depressor mandibulae muscles; (2) quantify the factors that contribute to high *in vivo* power output by estimating the elastic properties (i.e. displacement and stiffness) of the depressor mandibulae muscles and their series connective tissues; and (3) develop and test an elastic recoil model, based on *in situ* elastic properties of the depressor mandibulae muscles and series connective tissues, that accounts for the observed displacement, velocity, acceleration and power output during ballistic mouth opening *in vivo*. Whereas many studies have compared the elastic potential energy needed to power ballistic movements to that stored in elastic structures prior to movement (e.g. Alexander, 1968; Alexander and Bennet-Clark, 1977), the present study seeks not only to quantify the storage of elastic potential energy prior to movement, but also the contribution of elastic properties to the rate of energy recovery and power output.

Materials and methods

The depressor mandibulae muscles used in all experiments were similar in size: mean length=16.8 mm (range: 15.8–17.1 mm), mean mass=227 mg (range: 150–280 mg), and mean Physiological cross-sectional area (PCSA)=0.135 cm^2 (range: 0.092–0.165 cm^2). Experiments were performed at room temperature (22±2°C). To insure the welfare of the animals, all procedures were approved by Northern Arizona University's Institutional Animal Care and Use Committee.

Kinematic analysis of ballistic mouth opening

Adult Colorado River toads, *Bufo alvarius* Girard (*N*=4), were imaged digitally at 1000 Hz while feeding using a Redlake™ Motionscope high-speed digital imaging system with synchronized, stroboscopic, infrared illumination. A grid of 1 cm squares was used to calculate the scaling factor and aspect ratio. Toads were placed on a flat stage, oriented perpendicular to the camera, and allowed to feed unrestrained on adult crickets (*Acheta domesticus*, length=2.5 cm). The crickets were placed at varying distances from the toads (1–11 cm) to elicit variability in effort during prey capture behavior (see below). Three feeding sequences were recorded for each toad. Electrodes were implanted into the depressor mandibulae and levator mandibulae posterior longus muscles on the right and left sides, the toads were again imaged at 1000 Hz while feeding, and 11–22 sequences were obtained after implantation (total of 71 sequences from 4 individuals). After a series of feeding sequences synchronized with electromyograms had been recorded, the toads were prepared for *in situ* force-lever studies (see below). Feeding sequences were digitized using Didge 2.2 motion analysis software (A. Cullum, Creighton University, Omaha, NE, USA). For each frame, the digitized points included the upper jaw tip, jaw joint, lower jaw tip and prey item. Only the ballistic phase of mouth opening (i.e. first 20 ms of the prey capture sequence) was analyzed.

For each frame, the distance to the prey item (i.e. shortest distance from the lower jaw tip to prey) was calculated. Gape distance (i.e. distance between the upper and lower jaw tips) and gape angle (i.e. angle subtended by the upper and lower jaw tips with the jaw joint at the vertex) were computed using the Euclidean distance and the law of cosines, respectively. The total distance shortened by the depressor mandibulae muscles during the ballistic phase was calculated by dividing the gape distance by the in-lever/out-lever ratio of the muscle. The position data were smoothed using a heptic spline function (QuickSAND) (Walker, 1998). Instantaneous velocity (v) and acceleration (a) were estimated as the first and second derivatives of the smoothed position data for each 1 ms time step. For each feeding sequence, peak instantaneous power was calculated as:

$$P = m_{\text{eff}} v a \,, \tag{1}$$

where m_{eff} is the total effective mass (see Anatomical measurements, below). The work done by the depressor mandibulae muscles during ballistic mouth opening was estimated as the time integral of the instantaneous positive power using a customized Matlab (version 7.0.0) program.

The general equation of motion for a damped mass–spring system is:

$$F_{\text{t}} = m_{\text{eff}} \ddot{x}_{\text{t}} + b_{\text{eff}} \dot{x}_{\text{t}} + k_{\text{t}} x_{\text{t}} \,, \tag{2}$$

where: F_{t}=total force, m_{eff}=effective mass, b_{eff}=effective damping coefficient, x_{t}=total displacement and k_{t}=total spring constant. The time solution $x_{\text{t}}(t)$ for the general equation can be obtained arithmetically using the characteristic equation method for the under-damped case:

$$x_{\text{t}}(t) = e^{-\zeta \omega_{\text{n}} t} \left[x_0 \cos(\omega_{\text{d}} t) + \left(\frac{v_0 + \omega_{\text{n}} x_0}{\omega_{\text{d}}} \right) \sin(\omega_{\text{d}} t) \right], \tag{3}$$

where ω_n is the natural frequency of vibration, ζ is the damping ratio, and ω_d is the damped frequency of vibration:

$$\omega_n = \sqrt{k_t / m_{eff}}\,, \quad (4)$$

$$\zeta = b_{eff} / 2m_{eff}\omega_n\,, \quad (5)$$

$$\omega_d = \sqrt{1 - \zeta^2}\omega_n\,. \quad (6)$$

For each feeding trial, Berkeley Madonna (version 8.0.1) was used to find the values of the non-linear spring constant (k_t) and effective damping coefficient (b_{eff}) that minimized the squared difference between the position predicted from the time solution of the general equation of motion for a damped mass-spring system (Eqn. 2) and the observed kinematic data [initial displacement x_0 and the total displacement over time $x_t(t)$], given the m_{eff} estimated for each toad from anatomical measurements and initial velocity (v_0)=0.

Electromyography

Electromyograms were recorded from the depressor mandibulae muscles and the largest of the six jaw adductor muscles, the levator mandibulae posterior longus, on the right and left sides of four toads (Ba 1–4). Bipolar hook electrodes were constructed from 0.05 mm diameter formvar-coated stainless steel wire (California Fine Wire Co., Grover Beach, CA, USA) with bared tips (0.5 mm). The dipole spacing of the electrodes was ~1 mm. Toads were anesthetized in a solution of tricaine methanesulfonate (MS-222) (0.1 g l^{-1} water) buffered to a pH of 7.0 using sodium bicarbonate. Incisions (~0.5 cm) were made to expose the jaw muscles. Using a 23-gauge hypodermic needle, the tips of the electrodes were implanted into the belly of each muscle. Electrode leads were threaded under the skin to the back of the toad, where they were sutured to the skin using 6.0 surgical silk. The leads were connected to a differential AC amplifier (A-M Systems, model 1700, Everett, WA, USA).

Analog signals were band-passed (10–5000 Hz), notch-filtered at 60 Hz, amplified (1000×), and digitized at 4000 Hz (Peak Performance Technologies, Inc., Centennial, CO, USA). The signals were later high-pass filtered at 300 Hz to remove low-frequency motion artifacts. The onset of EMG activity was defined as the time at which the EMG amplitude rose above twice the mean baseline voltage. Likewise, the muscle was considered to be electrically inactive when the EMG amplitude fell below twice the mean baseline voltage. EMG recordings were synchronized with digital images (1000 Hz). For each trial, the peak amplitude (mV), duration (ms), and full-wave rectified, integrated area (mVs) of EMG activity that occurred prior to the onset of mouth opening were calculated. For each toad, the relationships between EMG activity (i.e., duration, peak amplitude, rectified integrated area), prey distance (cm), and total displacement (x_t) were examined (Pearson product–moment correlation coefficients, P=0.05). For two toads (Ba 1 and 3), the amplitude of the EMG signal declined significantly over time (P<0.05), so only the duration data were analyzed.

In situ force-lever experiments

A dual servo-motor force lever (Aurora Scientific, Inc., Series 305B, Aurora, ON, Canada) was used to examine the contractile and elastic properties of the depressor mandibulae muscles. For each muscle, a maximum isometric tetanic contraction was performed, followed by an after-loaded force–velocity experiment (N=3), a length–tension experiment (N=3), or a load-clamp experiment (N=3; Ba 1–3).

Toads were cooled in a refrigerator at 4°C for 1 h and double-pithed prior to each force-lever experiment. On the temporal aspect of the cranium, the depressor mandibulae muscles lie under the parotid glands, which in toads secrete a moderately potent toxin. To avoid contact between toxic parotid gland secretions and the muscle tissue, secretions were squeezed from the parotid glands with paper towels prior to removal of the skin and connective tissue overlying the depressor mandibulae muscles. We used an *in situ* preparation that maintained the muscle's natural origin, insertion, and line of action (Fig. 1A). This procedure also avoided trauma to the muscle's blood supply, which remained intact. The mandible was transected ⩽5 mm anterior of the jaw joint and freed of its attached hyolingual musculature. All muscles that resist joint rotation due to shortening of the depressor mandibulae muscle (i.e. jaw adductors) were removed (Fig. 1B), and it was assumed that resistance to joint rotation was negligible. During experiments, the muscle was irrigated frequently with amphibian Ringer's solution (6 g NaCl, 0.075 g KCl, 0.1 g $CaCl_2$, and 0.1 g $NaHCO_3$ l^{-1} H_2O).

The depressor mandibulae muscle inserts on the retroarticular process *via* a small aponeurosis (i.e. a broad, flat tendon <1 mm long in all specimens). Spider Wire™ microfilament (Johnson Worldwide Associates, Inc., Sturtevant, WI, USA) was pushed through the insertion of the

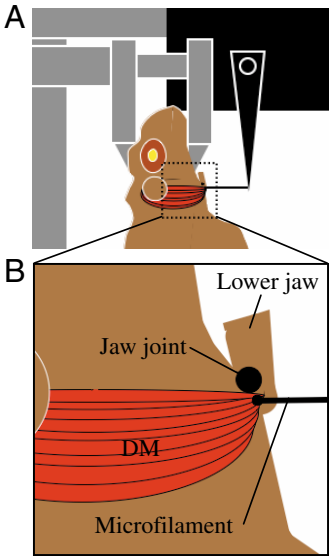

Fig. 1. (A) Force-lever setup and (B) *in situ* jaw–joint preparation for measurement of contractile and elastic properties of the depressor mandibulae muscles.

depressor mandibulae at the tip of the retroarticular process and tied off securely (Fig. 1B). A loop was tied at the free end of the microfilament so that its total length from the muscle insertion to the arm of the force lever was 2.5 cm. The cranium of the toad was fixed to a metal frame with a steel clamp, and the frame was mounted on an aluminum vibration-resistant table (Fig. 1A). The animal was clamped rostral end up, so that the line of pull of the depressor mandibulae on the lever arm was in the horizontal plane, thus minimizing effects of gravity on the lever. The looped end of the microfilament was placed into a notch on the arm of the force lever.

The viscoelastic properties of Spider Wire™ were investigated by performing load-clamp tests on 2.5 cm lengths of Spider Wire alone. The Spider Wire™ was loaded with forces of 4.0–5.1 N, which were reduced rapidly to 2.8–1.0 N. When the force was reduced, there was a small step decrease in the length of the Spider Wire with no observable oscillations. Over the range of loads used in this study, the decrease in length was independent of clamp load (N=5 trials, r^2=0.06), and averaged 0.06 mm. The contribution of the Spider Wire, including its connections to muscle and lever, to the total displacement during load-clamp experiments was 0.35–0.37% of muscle resting length.

Force-lever experiments were performed with the depressor mandibulae muscle at its *in vivo* resting length (Fig. 2), which corresponds to the length at which its active force production is greatest (L_0). The resting length is the greatest length that the depressor mandibulae muscles can attain *in vivo* because, at this length, the mouth is fully closed. When the muscle insertions were isolated initially, the muscles assumed a length that was shorter than their *in vivo* resting length by ~1 mm (6% *ML*). Using the lever, the length of the muscles was increased slowly until the passive tension was 0.1 N (7–11 mN mm^{-2}). At this passive tension, the length of the muscles corresponded to the *in vivo* resting length, as measured to the nearest 0.1 mm with digital calipers prior to isolation. The contribution of the passive muscle strain (i.e. at resting length and a passive tension of 0.1 N) to the total displacement during the load-clamp experiments was calculated from the passive length–tension curve as the strain at a passive force of 0.1 N minus the strain at the *in situ* load (0.03–0.08 N).

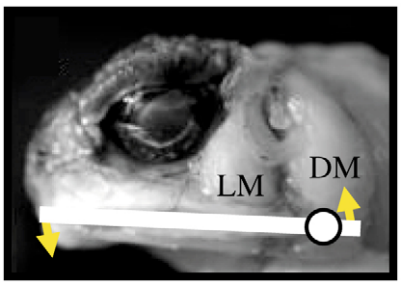

Fig. 2. Cranium and lower jaw of *Bufo* showing the mouth-opening muscle (depressor mandibulae=DM) and the largest of the mouth-closing muscles (levator mandibulae posterior longus=LM). The jaw joint is indicated by a white circle, and the in- and out-levers are indicated by white bars. Contraction of the depressor mandibulae (upward arrow) produces rotation of the lower jaw about the joint (downward arrow).

For stimulation, two electrodes (diameter 0.076 mm) were implanted into the denervated depressor mandibulae muscle. To achieve maximum activation, 5 mm of each electrode tip was bared of insulation, and the electrodes were inserted into the muscle belly so that the distance between them was half the total muscle length (e.g. a 20 mm muscle would have electrodes implanted 5 mm from the origin and 5 mm from the insertion, spaced 10 mm apart). The electrodes were attached to a Grass SIU5 Isolation Unit in series with a Grass S48 Stimulator. The voltage needed to produce maximum activation was determined using twitch contractions (1 ms pulse duration), and this voltage was increased by 20% in subsequent tests (i.e. supramaximal voltage). Supramaximal voltage ranged from 80–120 V. Tetanic stimuli were delivered in single trains of 400 ms duration at a frequency of 80 pulses s^{-1}. To avoid fatigue, the muscles were rested for 15 min between trains. In these experiments, maximum isometric force never fell below 22 N cm^{-2}, which indicates that muscle recruitment was maximal and fatigue was minimal.

External load was controlled and length changes were measured (in after-load and load-clamp experiments) using the series 305B lever, which is capable of recording forces and excursions up to 5 N and 10 mm, respectively. The lever was tuned to factory specifications for minimal damping and step response time (2 ms) and was calibrated using weights of known mass. For data capture, the servo-motor output was sent to a GW Instruments InstruNet Model 100B A/D I/O System connected to a Macintosh 7200 computer running GW Instruments SuperScope II software sampling at 4000 Hz.

Contractile properties

To generate a length–tension curve for the depressor mandibulae muscles, each muscle (N=3) was stimulated isometrically over a series of 6–8 lengths at 0.5 mm increments. Stimulation parameters were as described above. From these experiments, we measured the passive, active and total tension at each length. To determine where on its length–tension curve the depressor mandibulae muscles operate *in vivo*, muscle length was measured to the nearest 0.1 mm with digital calipers with the mouth in the fully closed position, prior to isolation of the muscles.

To generate a force–velocity curve for the depressor mandibulae muscles, we performed a series of isotonic after-loaded contractions at 6–8 loads per muscle (N=3). From these data, force–velocity curves were generated and the maximum velocity of shortening, V_{max}, was estimated using Hill's equation (Hill, 1938):

$$(P + a)\,(v + b) = (P_0 + a)b\,, \qquad (7)$$

where P=force, P_0=maximum isometric force, v=velocity of shortening with asymptotes P=–a and v=–b. A Matlab (version 7.0.0) program using the lsqcurvefit function was used to find the values of the parameters (a and b) that minimized the

squared difference between the observed force–velocity data and the predictions of the Hill equation for each individual muscle.

Elastic properties

It is widely believed (e.g. Alexander and Bennet-Clark, 1977) that muscles themselves contribute little to the power of ballistic movements because muscles shorten slowly, relative to elastic recoil in tendon or cuticle, even under very low loads. This idea follows directly from Hill's force–velocity curve (Hill, 1938): the velocity of muscle shortening increases hyperbolically with decreasing load. Because power is the product of force and velocity, the force–velocity property of muscle necessarily limits power output. When the force is large, the velocity is small, and when the velocity is large, the force is small.

The apparent trade-off between force and velocity is, at least in part, an artifact of Hill's after-loaded isotonic paradigm for generating the force–velocity curve (Hill, 1938). In this paradigm, not only does the external load vary, but the duration of muscle stimulation prior to the onset of shortening also varies with the load. This means that the muscle is stimulated for very short durations (as little as 10–15 ms) at the smallest loads and for much longer durations (>250 ms) at the largest loads. Hill designed the after-loaded paradigm specifically to remove any contribution of muscle series elasticity to the observed shortening, in order to study the properties of the contractile elements (Hill, 1938). However, if muscles are activated for relatively long durations prior to shortening, as often occurs during natural movements, then recoil of series elastic elements within the muscle itself will contribute to power output. The question is, for a given duration of pre-movement activation, how much power can muscles produce as the load decreases?

For these reasons, we chose to quantify the elastic properties of the depressor mandibulae muscles using the load-clamp technique. The load-clamp experiments were designed to mimic the *in vivo* behavior of the depressor mandibulae muscles. *In vivo*, the depressor mandibulae muscles contract prior to mouth opening, producing strain in series elastic elements of the cranium and jaws, as well as within the muscle itself. When the mouth opens, the load decreases rapidly. In load-clamp tests, the load is reduced following isometric stimulation, which results in biphasic shortening of the muscle. An initial rapid change in length (due to recoil of series elastic elements within the muscle) is followed by a slower change in length (due to cyclic interactions of contractile proteins within the muscle). Damped oscillations appear during the transition (Fig. 3).

A series of load-clamp experiments (N=3; Ba 1–3) was performed to investigate the elastic recoil of the depressor mandibulae muscles during rapid unloading. *In vivo*, the depressor mandibulae muscles are activated for 50–250 ms prior to the onset of mouth opening (Monroy and Nishikawa, 2003). Guided by the delay between the onset of muscle activation and the onset of mouth opening that we observed *in vivo*, we performed load-clamp tests using three durations of muscle stimulation: 50, 100 and 200 ms. Load-clamp tests using stimulation durations of 50 and 200 ms were performed for the first two specimens immediately after EMG data were collected but before the data could be analyzed. Once we analyzed EMGs from these animals, we realized that toads seldom activate their depressor mandibulae muscles *in vivo* for less than 100 ms prior to mouth opening (only 3 of 71 feeding trials). Therefore, for the third toad, we performed load-clamp tests using stimulation durations of 100 and 200 ms. Fortuitously, these stimulation durations produced forces prior to the load clamp ranging from 1.0–3.4 N (see Fig. 12). The depressor mandibulae muscles reach maximum isometric tetanus in 233–273 ms.

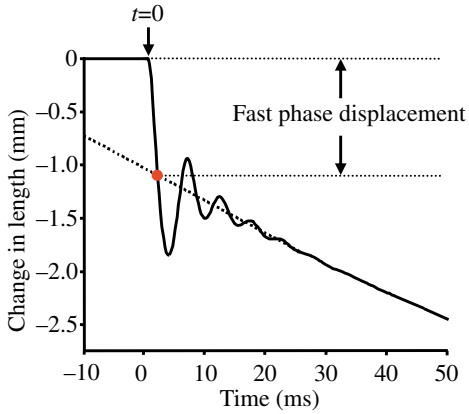

Fig. 3. Change in length of a depressor mandibulae muscle *vs* time during a load-clamp experiment. When the load is reduced (t=0), the muscle exhibits a fast phase of shortening and a slow phase of shortening with oscillations during the transition. To define the fast to slow phase transition (red circle), a line representing shortening during the slow phase, and bisecting the oscillations, was extrapolated back to its initial intersection with the length trace. Fast phase displacement is defined as the change in length that occurs from the initial position (t=0) to this point of intersection. This trace corresponds to Ba 1 (ΔF=2.82) in Fig. 8B.

For each muscle and duration of stimulation (50, 100 or 200 ms), the distance shortened during the fast phase (i.e. displacement, x_m), was measured over a series of 5–7 clamp loads. Each load-clamp trial was divided into a fast and a slow phase of shortening (Fig. 3). To accomplish this, the slope and intercept of the line that represents the slow phase shortening velocity, which also bisects the damped oscillations, was determined. This line then was extrapolated to the y-intercept (t=0). The end of the fast phase was defined as the first intersection between this line and the observed trace of muscle length *vs* time (Fig. 3).

Estimating strain in series elastic elements during depressor mandibulae stimulation

The goal of these experiments was to estimate the degree to which the depressor mandibulae muscles impose strains on series elastic structures of the cranium and lower jaw prior to

mouth opening. As for the force-lever experiments, toads (N=3) were cooled and double-pithed, and all jaw-adductor muscles were removed. The intact lower jaw was sutured to the maxilla to prevent mouth opening. The cranium was clamped to a metal frame on a vibration-resistant table, and stimulating electrodes were implanted in the depressor mandibulae muscle as described above. The depressor mandibulae muscle was stimulated supramaximally, and movements of the cranium and lower jaw were recorded digitally at 500 Hz. Points at the origin of the depressor mandibulae on the cranium, the insertion of the depressor mandibulae on the retroarticular process, and a fixed point on the clamp were digitized at 20 ms intervals (every tenth frame) beginning with the frame preceding the first perceptible movement. Total shortening of the depressor mandibulae muscle, as well as strain at the cranial insertion and retroarticular process, were measured as a function of time from the onset of movement. We assumed that the total shortening of the depressor mandibulae muscle is equal to the total strain in all extra-muscular structures combined (i.e. the sum of the strain at the muscle origin and insertion), and that strains in directions other than the direction of muscle shortening were negligible. Immediately after the *in situ* strain data had been recorded, each specimen was prepared as described above for the force-lever experiments. The muscle insertion was attached to the arm of the force lever, the muscle was stimulated tetanically until it reached its maximum isometric force, and the force was measured as a function of time from the onset of stimulation. For each depressor mandibulae muscle, the strain *vs* time and force *vs* time plots were aligned at t=0 to obtain the relationship between force and strain.

Anatomical measurements

The effective mass (m_{eff}) moved by the depressor mandibulae muscles *in vivo* was estimated as the mass of the lower jaw plus tongue, multiplied by the moment of this mass (i.e. distance from center of mass to center of rotation divided by distance from muscle insertion to center of rotation), plus the mass of the depressor mandibulae muscles and retroarticular processes. The effective mass ranged from 9.12–12.94 g in the four individuals for which *in vivo* kinematic data were collected (Ba 1–4). The *in vivo* inertial load ($m_{\mathrm{eff}}\boldsymbol{g}$) was estimated as the effective mass multiplied by the acceleration due to gravity ($\boldsymbol{g}$). Because the load is distributed over the right and left depressor mandibulae muscles arranged in parallel, the *in vivo* loads (mean=0.1 N) represent only 1.3–1.8% of the maximum isometric force that the two depressor mandibulae muscles can produce (~5–8 N).

To estimate total shortening of the depressor mandibulae muscles and associated connective tissues during ballistic mouth opening, gape distances measured from digital images were converted to total shortening distances using the in-lever/out-lever ratio (i.e. distance from muscle insertion to center of rotation divided by distance from center of rotation to tip of the lower jaw). The lower jaw was dissected from the specimen and cleaned to reveal the anatomy of the jaw joint and retroarticular process. Measurements used for in-lever/out-lever calculations were taken from digital images of the dorsal surface of the isolated lower jaw as straight line distances parallel to the longitudinal axis of the head. We assumed that the center of rotation of the lower jaw is at the center of the jaw joint itself. The in-lever/out-lever ratio ranged from 1:7.7–1:8.6 in the four individuals used in this part of the study. The shortest (deepest) and longest (most superficial) distances along the muscle surface from origin to insertion were measured with digital calipers, and the mean of these distances was used to calculate strain (*ML*) and strain rate (*ML* s^{-1}).

Sarcomere length

Sarcomere lengths of the depressor mandibulae muscle at resting length were measured from specimens (N=3) prepared for transmission electron microscopy using standard techniques (e.g. Nishikawa et al., 1999). To ensure that the muscles maintained their natural position during fixation, the entire posterior half of the head and lower jaw (from the eye to the jaw joint) was submerged in fixative (6.25% glutaraldehyde in sodium cacodylate buffer, pH=7.4). The mouth was sutured shut to ensure that the muscle maintained its resting length during fixation. Sarcomere lengths were measured from digital images taken from four regions within the muscle: superficial belly, deep belly, origin and insertion. For each region in each muscle, ten sarcomeres were measured from at least two different micrographs in three toads (N=120). A two-way factorial ANOVA was used to test the effects of region within the muscle (fixed) and individual (random) on sarcomere length.

Elastic recoil model of ballistic mouth opening in toads

In order to account for the power output of the depressor mandibulae muscles during ballistic mouth opening, we developed an elastic recoil model of the toad cranium and jaws (Fig. 4). In the model, each depressor mandibulae muscle (Fig. 4, red symbols) is represented as a force generator (i.e. cross bridges) in series with a spring (i.e. series elastic component of the muscle). Extra-muscular connective tissues at the origin and insertion are represented together as a single spring in series with the muscle (Fig. 4, blue symbols). The springs originate on the cranium and suspend an effective mass (m_{eff}) equal to the product of the mass of the lower jaw plus tongue and its moment plus the mass of the depressor mandibulae muscles and retroarticular processes. Dashpots (Fig. 4, purple symbols) represent the total effective damping (b_{eff}) of the feeding apparatus. When the depressor mandibulae muscles become active prior to mouth opening, they store elastic potential energy in both intramuscular (red) and extra-muscular (blue) springs. When the mouth opens rapidly, the springs return to their equilibrium position (x_{t}) at a rate that depends on the total stiffness (k_{t}), effective mass (m_{eff}), and effective damping coefficient (b_{eff}). Given the anatomical arrangement of the various spring elements (Fig. 4), the

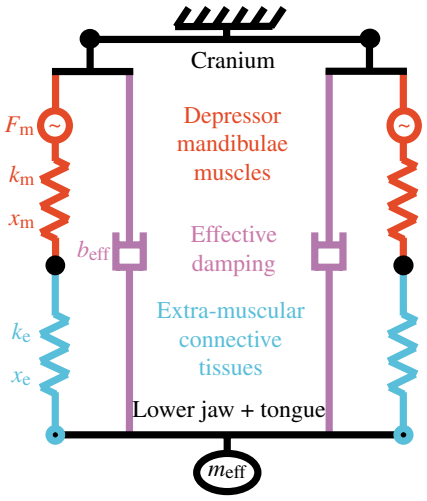

Fig. 4. Elastic recoil model of the toad cranium. The model includes the pair of depressor mandibulae muscles, which originate on the cranium (ground) and insert on the retroarticular processes of the lower jaw. Each muscle (red) was modeled as a force generator (i.e. cross bridges) and a spring (i.e. series elastic component) arranged in series. On each side of the cranium, the depressor mandibulae muscle is arranged in series with an extra-muscular spring element (blue) that represents the sum of all extra-muscular structures that are strained by contraction of the depressor mandibulae prior to movement (i.e. cranium and retroarticular process). The effective mass (m_{eff}) is suspended from these springs. Effective damping (b_{eff}) of the mass-spring system is depicted in purple.

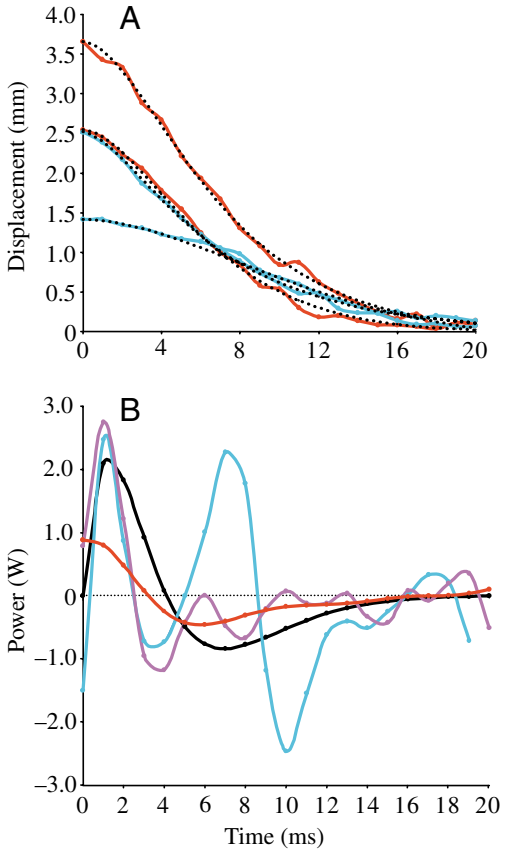

Fig. 5. (A) Fit between observed and predicted displacement (x_t) *vs* time. Displacements from two trials (high effort and low effort) are shown for two toads. Colors represent different individuals. For each toad (N=4), effective mass (m_{eff}) was estimated from anatomical data. For each feeding trial (N=71), total displacement (x_t) *vs* time was estimated from digital images. The time solution for the general equation of motion (Eqn 3) was solved to find the values of the spring constant (k_t) and damping coefficient (b_{eff}) that provided the best fit (dotted black lines) to the observed kinematic data. (B) Maximum instantaneous *in vivo* power output of the depressor mandibulae muscles and series connective tissues during ballistic mouth opening. Colors represent different individuals.

expressions for the total displacement (x_t) and total stiffness (k_t) are as follows:

$$x_t = x_e + x_m \,, \tag{8}$$

$$k_t = 2[(1/k_m + 1/k_e)^{-1}] \,. \tag{9}$$

To implement the model, the non-linear, load-dependent displacements (x_m) and spring constants (k_m) of the depressor mandibulae muscles at *in vivo* loads were estimated from load-clamp data. The displacement (x_e) and spring constant (k_e) of the extra-muscular connective tissues were estimated from *in situ* muscle stimulation experiments. Eqn 8 and 9 were used to calculate the total spring constant (k_t) at the *in vivo* load that corresponds to a given total displacement (x_t) and total force (F_t). For a given total force (F_t), the total spring constants (k_t) predicted by the model were compared to the total spring constants (k_t) estimated from kinematics as described above.

Results

Kinematic analysis of in vivo ballistic movements

During the fast (i.e. ballistic) phase, the mouth opens rapidly to angles of up to 60° in less than 20 ms. The gape distances achieved during ballistic mouth opening varied among feeding trials for each individual (Fig. 5A, Table 1). Maximum gape distances ranged from 19.1–28.3 mm. Corresponding maximum total displacements of the depressor mandibulae and series connective tissues (x_t) ranged from 2.5–3.7 mm (Table 1). Peak instantaneous velocity and acceleration of the center of mass of the lower jaw and tongue ranged from 0.71–1.00 m s^{-1} and 198–789 m s^{-2}, respectively (Table 2). Peak instantaneous power output, calculated from kinematics using Eqn 1, is achieved within the first 1–2 ms after the onset of mouth opening (Fig. 5B) and ranged from 0.9 to 4.1 W (Table 2). Peak instantaneous muscle mass-specific power output ranged from 2.7 to 9.6 W g^{-1} (Table 2). The time integral of positive instantaneous power is equal to the total work performed by the depressor mandibulae muscles during ballistic mouth opening. For the trial with the maximum mass-specific power output (9.6 W g^{-1}, Table 1), the total work was 4.3 mJ.

The total spring constant (k_t) and effective damping coefficient (b_{eff}) were estimated by fitting the raw kinematic data to the time solution (Eqn 3) of the general equation of

Table 1. *Results from kinematic analysis of the ballistic phase (first 20 ms) of mouth opening in freely behaving toads*

			Gape distance (mm)	x_t (mm)			r^2
Individual	In:out lever ratio	*N*	Max/Min	Max/Min	k_t (N m^{-1})	b_{eff} (Ns m^{-1})	Max/Min
1	1:7.9	11	28.3/19.2	3.7/2.5	712±73	5.6±0.6	0.998/0.981
2	1:7.9	22	23.9/18.7	3.1/2.4	582±28	4.4±0.2	0.999/0.989
3	1:8.6	22	19.1/11.0	2.5/1.4	522±40	4.1±0.3	0.998/0.989
4	1:7.7	16	24.8/22.5	3.6/2.9	508±42	4.4±0.3	0.999/0.989
Mean	1:8.0	–	24.0/17.9	3.2/2.3	581	4.6	0.999/0.987
s.e.m.	0.2	–	1.9/2.4	0.3/0.3	47	0.3	0.0003/0.002

Values for k_t and b_{eff} are means ± s.e.m. For individual and in:out lever ratio of the depressor mandibulae muscles, *N*=4; listed *N* values = number of feeding trials per individual.

x_t, total displacement of the depressor mandibulae muscles and extra-muscular connective tissues; k_t, mean total spring constant; b_{eff}, mean effective damping coefficient; r^2, least-squares fit [between observed and predicted total displacement (x_t) *vs* time].

motion for a single degree-of-freedom damped mass-spring system. Mean values of k_t for each toad ranged from 508 to 712 N m^{-1} (Table 1). Mean values of b_{eff} ranged from 4.1 to 5.6 Ns m^{-1} (Table 1), which correspond to damping ratios of 85.7–108.5% (mean=94.5%). Eqn 2 produced good fits to the experimental data. For 71 trials from four toads, r^2 ranged from 0.981–0.999 (Table 1, Fig. 5A).

Electromyography

The depressor mandibulae and levator mandibulae muscles exhibited bilaterally symmetrical activity when crickets were captured at distances ranging from 1–11 cm. The depressor mandibulae muscles consistently exhibited a biphasic activity pattern, with a first large burst that began 49–247 ms before the onset of mouth opening (Fig. 6A, Table 3). Ballistic mouth opening begins at the end of the first burst, and is followed by a second, shorter burst of activity associated with prey transport. Prior to mouth opening, the levator mandibulae posterior longus showed low amplitude activity (~20%) relative to its activity during mouth closing (Fig. 6A).

Two toads showed a significant positive association between total displacement (x_t) and total integrated area of depressor mandibulae activity preceding mouth opening (Fig. 6B,C, all P<0.05, r^2=0.22–0.27). These results are consistent with the hypothesis that the total displacement (x_t) of the depressor mandibulae muscles and series connective tissues increases with the force (F_t) that develops in the depressor mandibulae muscles prior to movement. All four toads showed a significant positive association between the duration of depressor mandibulae activity preceding mouth opening and the distance to prey (Fig. 6D, all P<0.05, r^2=0.26–0.66), suggesting that the muscles are activated earlier, relative to the onset of mouth opening, when prey are farther away.

Contractile properties of the depressor mandibulae muscles

At resting length, the depressor mandibulae muscles of toads (*N*=3) are also at their optimum length, L_0 (Fig. 7A). The slack length of the depressor mandibulae muscles is ~1 mm less than their resting length. Stretching the muscles to their resting length produced a passive tension of 0.1 N (7–11 mN mm^{-2}, ~2.5% P_0). Below L_0, both active and passive tension decline rapidly. Above L_0, active tension decreases rapidly, but total tension increases rapidly due to the increase in passive tension.

The force–velocity relationship of the depressor mandibulae muscles was determined *in situ* from a series of isotonic after-loaded contractions (Fig. 7B). V_{max}, estimated by fitting the raw force–velocity data to the Hill equation, ranged from

Table 2. *Results from kinematic analysis of the ballistic phase (20 ms) of mouth opening in freely behaving toads*

					Power (W)	Power (W g^{-1})
Individual	m_{eff} (g)	*N*	Velocity (m s^{-1})	Acceleration (m s^{-2})	Max/Min	Max/Min
1	9.12	11	1.00/0.76	290/204	1.3/0.7	2.7/1.4
2	9.94	22	0.83/0.69	500/183	4.1/0.6	9.6/1.3
3	9.33	22	0.78/0.21	198/2.5	0.9/0.04	2.9/0.1
4	12.94	16	0.71/0.48	789/98	2.5/0.3	5.2/0.6
Mean	10.33	–	0.83/0.54	444/122	2.2/0.4	5.1/0.9
s.e.m.	0.89	–	0.06/0.12	131/46	0.7/0.2	1.6/0.3

m_{eff}, total effective mass.

Individual (*N*=4), listed *N* values = number of feeding trials per individual, peak instantaneous velocity, peak instantaneous acceleration, peak instantaneous power output, and peak instantaneous mass-specific power.

3.5–3.7 *ML* s^{-1} (58.9–63.9 mm s^{-1}), with a mean of 3.6 *ML* s^{-1} (*N*=3). The maximum shortening velocity of the depressor mandibulae is both absolutely and relatively much slower (by a factor of ~4) than the shortening velocity of frog limb muscles (V_{max}~12 *ML* s^{-1}) (Lutz and Rome, 1994; Lutz and Rome, 1996). The maximum shortening velocity is sufficiently low that, even unloaded, the depressor mandibulae muscles are predicted to shorten by no more than 0.07 *ML* (1.2 mm) in 20 ms.

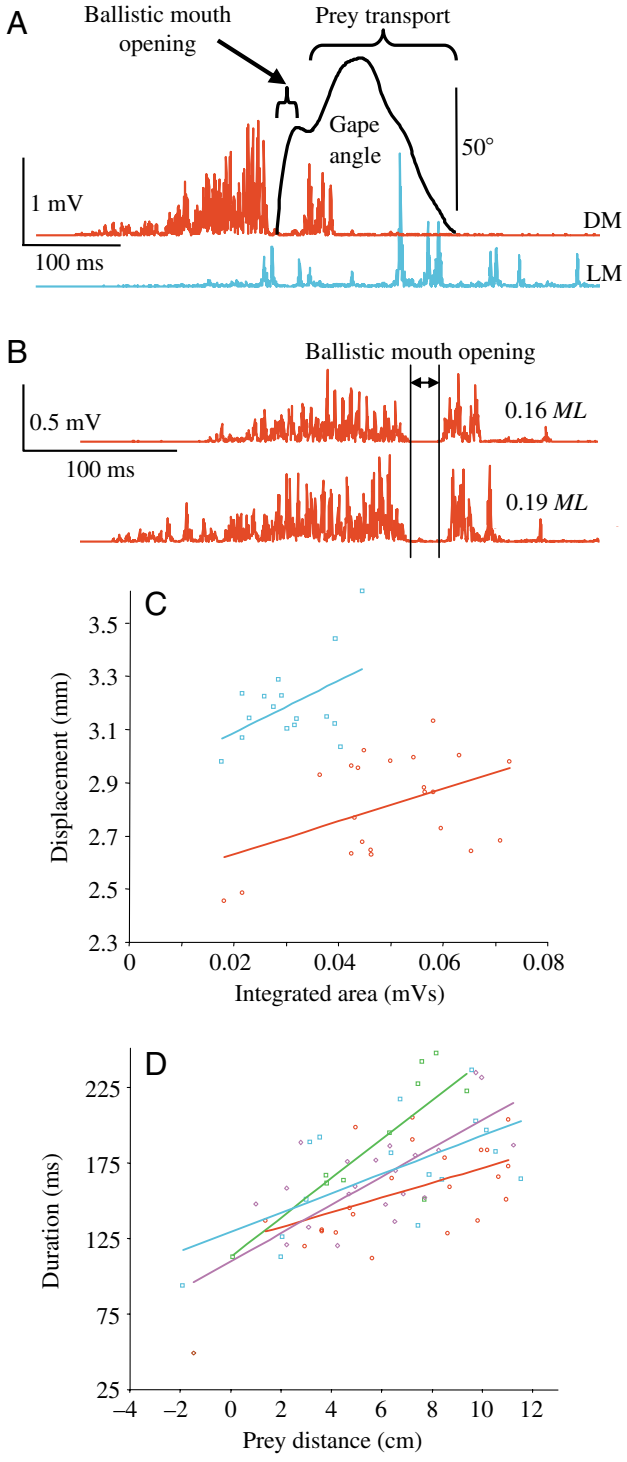

Table 3. *Amplitude, duration and integrated area of EMG activity in the depressor mandibulae muscles preceding mouth opening*

		Amplitude (mV)	Duration (ms)	Integrated area (Vs)
Individual	*N*	Max/Min	Max/Min	Max/Min
1	11	–	247/91	–
2	22	1.6/0.6	232/125	0.034/0.015
3	22	–	235/49	–
4	16	1.9/0.8	236/94	0.042/0.017

N = number of feeding trials per individual.

Elastic properties of the depressor mandibulae muscles

Load-clamp experiments were used to investigate the elastic properties of the depressor mandibulae muscles during elastic recoil. Original records for the load-clamp experiments in which the muscle was activated isometrically for 200 ms prior to load reduction are shown in Fig. 8A,B. From these records, the distance shortened during the fast phase was calculated for each load-clamp trial as described above (see Fig. 3). The maximum displacements (x_m) obtained *in situ* using the force lever were 2.6 mm (15.3% *ML*), 3.0 mm (17.5% *ML*), and 2.5 mm (15.3% *ML*), corresponding to changes in force (ΔF) of 3.27 N, 3.34 N and 2.45 N, respectively (Fig. 8B, Table 4).

The load-clamp experiments demonstrate that the depressor mandibulae muscles behave as non-linear springs in which muscle displacement (x_m) during elastic recoil increases

Fig. 6. (A) Gape profile during prey capture (black line) synchronized with EMG activity of the depressor mandibulae (DM, red) and levator mandibulae posterior longus (LM, blue). The ballistic phase of mouth opening is completed during the first 20 ms and is followed by slower mouth opening as the prey item is transported into the oral cavity. The depressor mandibulae exhibits a large burst of activity that precedes the onset of movement by up to 250 ms, and a smaller burst that accompanies the increase in gape angle during prey transport. The levator mandibulae shows low-level activity before movement, followed by a large-amplitude burst during mouth closing. Neither muscle is active during ballistic mouth opening. (B) Examples of depressor mandibulae activity during a trial with a smaller total displacement (x_t=2.8 mm, 0.16 *ML*, above) *vs* a trial with a larger total displacement (x_t=3.3 mm, 0.19 *ML*, below). Both trials are from the same toad (Ba 2). During the trial with the larger total displacement, the depressor mandibulae exhibits greater amplitude and a longer duration of activity prior to movement than during the trial with the smaller total displacement. Vertical lines delineate the ballistic phase of mouth opening. (C) Relationship between total integrated area of depressor mandibulae activity (mVs) preceding movement and total displacement (mm) during ballistic mouth opening (*N*=2). (D) Relationship between distance to prey (cm) and duration of depressor mandibulae activity prior to movement (*N*=4). Colors represent different individuals.

exponentially with the change in load $\Delta F=F_{before}-F_{after}$. The shape of the exponential functions:

$$x_m = 10^{(\Delta F - c_1)/c_2} \quad (10)$$

is described by two arbitrary constants, c_1 (N) and c_2 (kg s^{-2}). For each series of load-clamp trials, coefficients c_1 and c_2 were chosen to best fit the observed force–displacement data (Fig. 9A). Eqn 10 produced good fits to the observed force-displacement data in all six series of load-clamp trials ($0.973 \leqslant r^2 \leqslant 0.997$; Fig. 9A).

The non-linear spring constant of the muscles, k_m, is given by the first derivative of the inverse of Eqn 10 [$\Delta F=c_1+c_2\log(x_m)$]:

$$k_m = c_2 / (2.303 x_m) . \quad (11)$$

As x_m approaches 0, k_m approaches infinity, so the exponential model is not valid when ΔF is small. During elastic recoil, the stiffness (k_m) of the depressor mandibulae muscles decreases rapidly and non-linearly as the change in force during unloading (ΔF) increases (Fig. 9B). The stiffness (k_m) decreases as ΔF increases because the displacement (x_m) increases exponentially with ΔF.

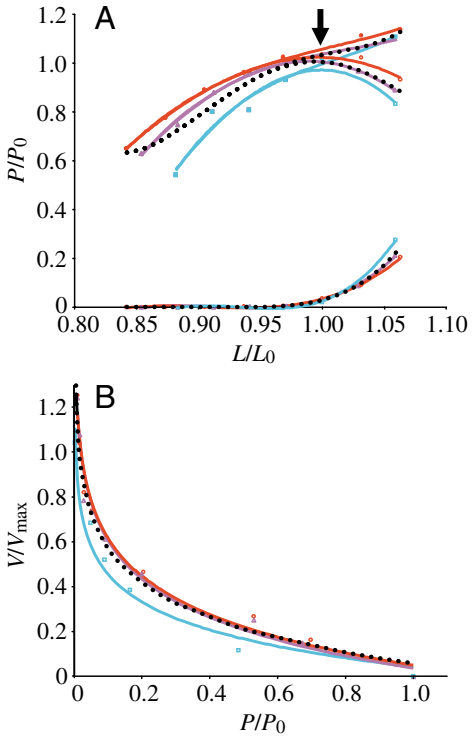

Fig. 7. (A) Length–tension curves for the depressor mandibulae muscle (N=3). At resting length (arrow), the muscle is at its optimum length (L_0), and a small amount of passive tension (~0.1 N) is present. Below resting length, active and passive tension decline rapidly. Colors represent different individuals (lines are best least-squares fit to third-order polynomials). Black dotted line represents mean for all individuals combined. (B) Force–velocity curves for the depressor mandibulae muscle (N=3). For the three individuals, V_{max} was 3.74, 3.62, and 3.48 $ML\ s^{-1}$. P=observed force, P_0=maximum isometric force, V=observed velocity, V_{max}=maximum shortening velocity. Colors represent different individuals (lines are best least-squares fit to Eqn 7). Black dotted line represents mean for all individuals combined.

Table 4. *Force-lever experiments: maximum isometric force, maximum stress and maximum displacement during load-clamp experiments*

		Isometric force (N)	Stress (N cm^{-2})	x_m	
Individual	N	Max/Min	Max/Min	(mm)	(% ML)
1	7	4.0/3.2	29.5/24.2	2.6	15.3
2	6	3.6/3.4	29.5/27.4	3.0	17.6
3	6	2.5/2.2	28.3/25.3	2.5	15.3
Mean	–	3.4/2.9	29.1/25.6	2.7	16.1
s.e.m.	–	0.5/0.4	0.4/0.9	0.1	0.8

x_m, maximum displacement.
N=number of trials per individual. (See Fig. 8B for raw data.)

During load-clamp experiments, ΔF can be controlled by varying either the duration of muscle stimulation (F_{before}) or the clamp load (F_{after}). However, *in vivo*, F_{after} is constant for a given toad at a given time, but toads can vary F_{before} (and therefore ΔF) by modulating the duration and/or amplitude of muscle activation prior to movement. In order to model ballistic mouth opening *in vivo*, the constants c_1 and c_2 from all six series of load-clamp experiments were regressed with F_{before} (Fig. 9C), so that the parameters x_m and k_m could be predicted for any value of ΔF as follows:

$$c_1 = 1.168 + 2.142 F_{before} , \quad (12)$$

$$c_2 = 0.263 + 0.504 F_{before} . \quad (13)$$

Linear functions produced good fits to the experimentally derived coefficients (r^2=0.959 and 0.929, respectively).

Lever artifacts

Due to the oscillatory artifacts introduced by the interaction between the muscle and the servo-controlled lever, previous workers (e.g. Huxley and Simmons, 1971; Ford et al., 1977) have questioned the usefulness of the load-clamp technique for understanding the viscoelastic properties of muscle. The oscillations in muscle length that follow the rapid decrease in load are caused by several factors,

Fig. 8. Original data from 200 ms load-clamp experiments. (A) Change in length, force and stimulation (black line) *vs* time for load-clamp trials at a high clamp force (2.60 N, blue lines) and a low clamp force (0.31 N, red lines). The depressor mandibulae muscles were stimulated isometrically for 200 ms before the load was reduced. (B) Original records of force (left) and change in length (right) *vs* time from load-clamp experiments (N=3 toads). Numbers to the right of the force traces indicate change in load (ΔF). Note that length traces (right) begin 200 ms after the onset of muscle stimulation.

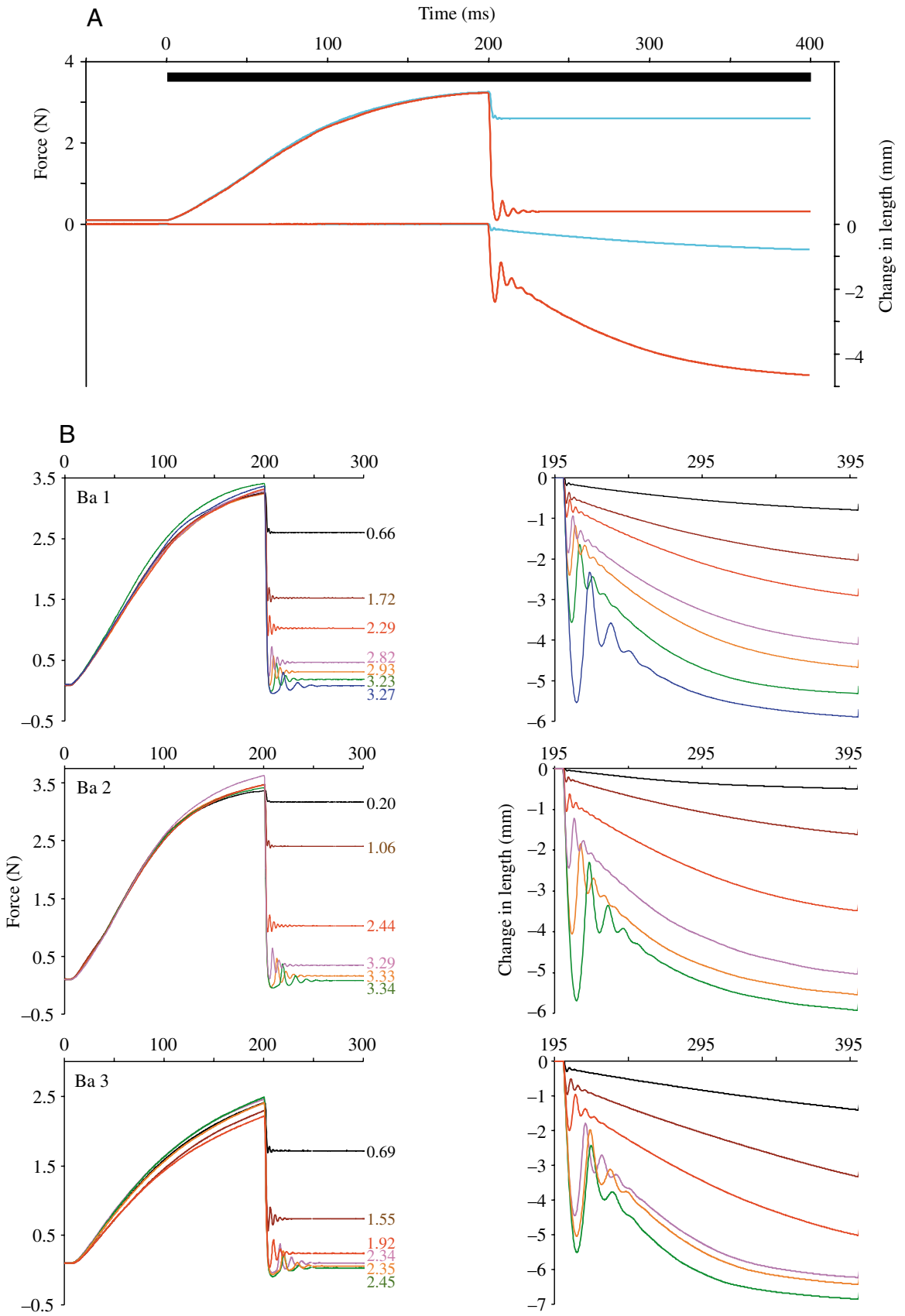

Fig. 8. For legend see previous page.

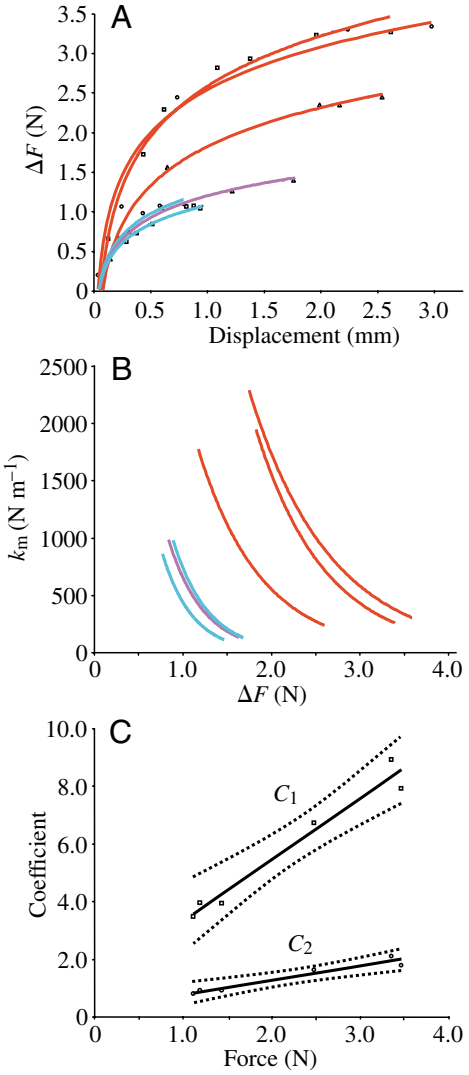

Fig. 9. Elastic properties of the depressor mandibulae muscles. Red lines: 200 ms muscle stimulation prior to load clamp (N=3). Blue lines: 50 ms muscle stimulation prior to load clamp (N=2). Purple line: 100 ms muscle stimulation prior to load clamp (N=1). (A) Change in force (ΔF) *vs* displacement (x_m) of the depressor mandibulae during load-clamp experiments. (B) Spring constant (k_m) as a function of the change in force (ΔF) during load-clamp experiments. (C) Linear regressions between coefficients c_1 (N) and c_2 (kg s^{-2}) and muscle force (N). The coefficients describe the shape of the exponential function relating x_m to ΔF (Eqn 9). Dotted lines show 95% confidence intervals for the regression slopes.

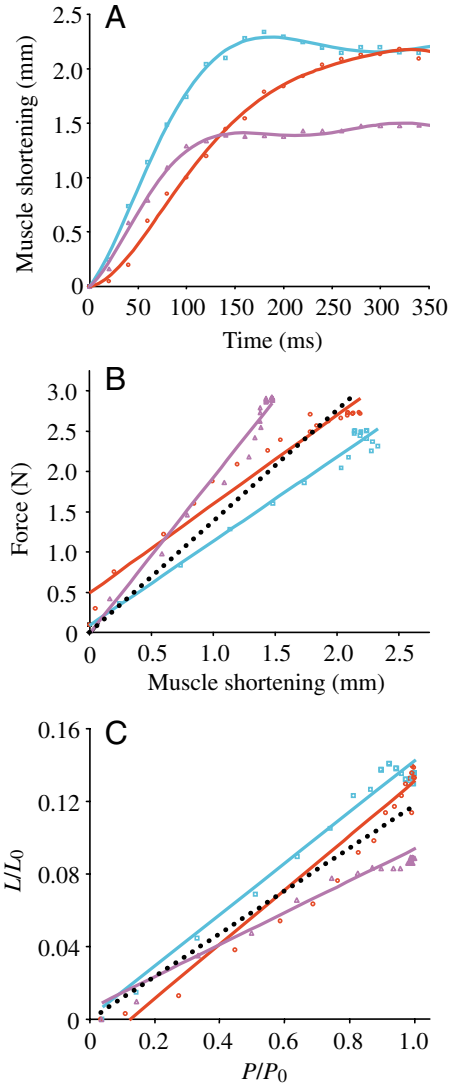

Fig. 10. Elastic properties of extra-muscular connective tissues. (A) Time course of depressor mandibulae shortening, which equals total stretch of extra-muscular connective tissues at the origin and insertion, measured using digital imaging during *in situ* muscle stimulation. (B) Depressor mandibulae force *vs* depressor mandibulae shortening. The slope is equal to the spring constant of the extra-muscular connective tissues (k_e), which averaged 1300 N m^{-1}. (C) Relative depressor mandibulae shortening (L/L_0) as a function of relative muscle force (P/P_0). Colors represent different individuals (N=3). Black dotted lines in B and C represent mean for all individuals combined.

including: (1) conversion of elastic potential energy to kinetic energy in the muscle, which causes it to overshoot its equilibrium position; (2) the inertia of the force lever itself; and (3) the interaction between the muscle and the servo-controlled force lever, which arises from the delay in the response of the lever to changes in force. In the experiments reported here, the lever was tuned to produce minimal damping (2 ms step response).

We used a modeling approach to estimate the contribution of lever artifacts to the observed fast phase displacement. To estimate the expected time-dependent shortening of the muscle itself (in the absence of lever artifacts), we again used the time solution (Eqn 3) of the general equation of motion for a damped mass-spring system. We modeled the expected shortening behavior of the depressor mandibulae muscle using the load-clamp trial with the greatest change in force (3.34 N, see Fig. 8B). For this trial, Eqn 3 was used to predict the expected time-dependent shortening behavior of the depressor mandibulae muscle (data not shown). The initial force, the change in force (ΔF), and the total fast phase

displacement (x_t) were used to calculate the muscle stiffness (k_m) at a given clamp load using Eqn 11. Berkeley Madonna (version 8.0.1) was used to find the value of the damping coefficient (b_{eff}) that produced the best fit between the model and the observed relationship between muscle length and time. This simple model, which assumes no lever artifacts, explained 95.4% of the observed variance in muscle length *vs* time (see Fig. 8B) in the load-clamp experiment with the largest oscillations and the greatest change in force. It explained a higher proportion of the variance in trials for which the change in force was smaller. This modeling approach shows that, taken together, all lever artifacts combine to produce an increase in the magnitude of the first oscillation, but they have no measurable effect on the natural period of vibration.

At the lowest clamp load, the effective damping of the muscle plus lever was 15% of critical damping (*vs* 94.5% *in vivo*, where additional factors contribute). The lower effective damping of the muscle plus lever system results in a small underestimate of the fast phase displacement. When the damping ratio is decreased from 94.5% to 15%, the trace of muscle length intersects the line representing slow phase shortening 10 ms earlier (see Fig. 3), thus decreasing the time allotted for fast phase shortening, and thereby decreasing the estimated fast phase displacement. The 10 ms decrease in the duration of fast phase shortening results in a decrease in fast phase displacement of 0.3 mm in a 17.0 mm muscle.

Estimating strain in series elastic elements during depressor mandibulae stimulation

During supramaximal depressor mandibulae stimulation *in situ*, the total strain of extra-muscular series elastic structures of the cranium and lower jaw ranged from 1.5 to 2.3 mm (8.9–14.1% *ML*) among the three specimens (Fig. 10A,C). Strain in the retroarticular process along the line of action of the depressor mandibulae ranged from 8.1 to 12% *ML*, with a mean of 10.6% (data not shown). Strain at the muscle's cranial origin ranged from 0.9 to 2.4% *ML* (data not shown).

For each muscle, data on shortening of the depressor mandibulae *vs* time, collected using *in situ* muscle stimulation with synchronous digital imaging, were combined with force *vs* time data from the same muscle, collected using the force lever, to produce estimates of the total strain in extra-muscular connective tissues as a function of muscle force (Fig. 10B). The force *vs* strain relationship was linear in two of three cases (Fig. 10B, pink and blue symbols), and was linear when data from all three specimens were pooled. The spring constant for all extra-muscular structures combined (k_e) was estimated as the slope of the linear relationship between total muscle shortening and force, constrained to pass through the origin. For any given force, the total strain in extra-muscular connective tissues (x_e) was estimated as the product of muscle length (l_m) and the linear function relating relative force (F_{rel}) to relative strain (measured as a proportion of muscle length).

The spring constant for all extra-muscular structures combined (k_e), estimated as the slope of the linear relationship between total muscle shortening and force (Fig. 10B), was 1300 N m^{-1} (range=1040–1865 N m^{-1}). The total strain (x_e) in all extra-muscular structures combined was estimated from the slope of the relationship between relative strain and relative force (Fig. 10C) with the intercept constrained to pass through the origin (Fig. 10C):

$$x_e = 0.118 l_m F_{rel} , \quad (14)$$

where l_m=muscle resting length and F_{rel}=relative force (P/P_0).

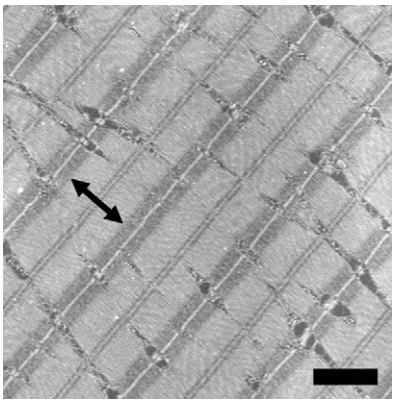

Fig. 11. Transmission electron micrograph of depressor mandibulae sarcomeres at resting (= optimal) length. The sarcomeres are short (~1.5 μm) compared to those of typical vertebrate skeletal muscles. The A-band (double-headed arrow) is also proportionately shorter (~1.0 μm) so that the relative overlap of thick and thin filaments is similar to that of a typical vertebrate skeletal muscle at L_0. Scale bar, 1 μm.

Sarcomere length

Transmission electron microscopy demonstrates that toad depressor mandibulae muscles at resting (=optimal) length have sarcomeres that are considerably shorter (1.5 μm) than is typical for sarcomeres of vertebrate skeletal muscle at L_0 (1.98–2.64 μm) (Burkholder and Lieber, 2001) (Fig. 11). The myosin filaments (A-band) are proportionately shorter (1.0 *vs* 1.6 μm) so that the relative degree of myofilament overlap is similar to that of a typical vertebrate sarcomere at L_0. Sarcomere length varied significantly among muscle regions (ANOVA: $F_{3,119}$=216.2, P<0.0001), although the difference among regions is relatively small. Sarcomere lengths (mean ± s.e.m.) were 1.52±0.015, 1.32±0.004, 1.44±0.004 and 1.49±0.007 μm in the superficial belly, deep belly, origin and insertion, respectively.

Elastic recoil model of ballistic mouth opening in toads

The purpose of the elastic recoil model was to account for the observed strain, shortening velocity, acceleration and power output of the depressor mandibulae muscles and series connective tissues during ballistic mouth opening. The model is based on the elastic properties of the muscles (measured *in situ* during load-clamp experiments, Eqn 10 and 11) and extra-muscular connective tissues (measured *in situ* during muscle

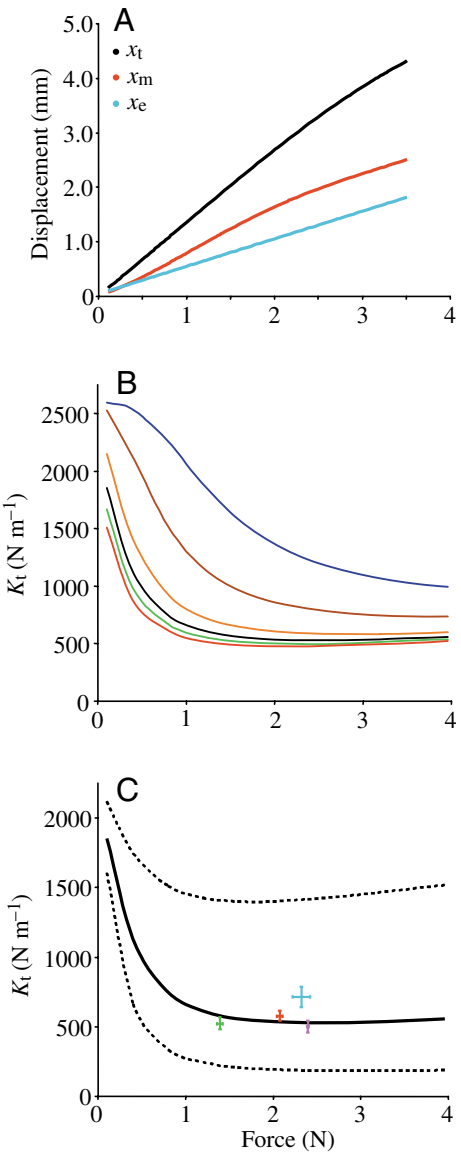

Fig. 12. (A) Displacement (x_m, x_e, x_t) predicted by the elastic recoil model as a function of the force developed by the depressor mandibulae muscles prior to movement. At all but the lowest forces (>0.25 N), the depressor mandibulae muscles (x_m) contribute more to total displacement (x_t) than the extra-muscular connective tissues (x_e). (B) Load-dependence of the relationship between depressor mandibulae force prior to movement (F_{before}) and total stiffness (k_t). The loads illustrated include 10 times the *in vivo* load (0.89 N, blue line), 5 times the *in vivo* load (0.45 N, brown line), twice the *in vivo* load (0.18 N, yellow line) and the observed *in vivo* load (0.09 N, black line), half the *in vivo* load (0.045 N, green line), and one tenth the *in vivo* load (0.009 N, red line). (C) Observed *vs* predicted relationship between the depressor mandibulae force prior to movement (F_{before}) and total stiffness (k_t). The solid line shows the total stiffness predicted by the elastic recoil model at the *in vivo* load. Dotted lines represent the 95% confidence interval. Colored symbols show the observed relationship between depressor mandibulae force prior to movement (F_{before}) and total stiffness (k_t) for each individual toad (mean ± s.e.m.) estimated by fitting the observed kinematic data to Eqn 3.

stimulation experiments, Eqn 14), in the context of their anatomical arrangement (Fig. 4, Eqn 8 and 9).

The paired depressor mandibulae muscles originate on the cranium and insert on the retroarticular processes of the lower jaw (Fig. 4). Each muscle was modeled as a force generator and a spring arranged in series (red symbols). On each side of the cranium, the depressor mandibulae muscle is arranged in series with a spring element that represents the sum of all extra-muscular structures that are strained by contraction of the depressor mandibulae prior to movement (i.e. cranium and retroarticular process). The springs on the left and right sides of the cranium are arranged in parallel and, from these, the effective mass is suspended (Fig. 4).

Given these anatomical arrangements, the total displacement (x_t) is equal to the sum of the displacements of the muscle spring (x_m) and connective tissue spring (x_e) arranged in series on each side of the cranium (Eqn 8). Substituting the experimentally derived expressions for x_m (Eqn 10) and x_e (Eqn 14) gives the expression for the predicted total displacement (x_t):

$$x_t = 10^{(\Delta F - c_1)/c_2} + 0.118 l_m F_{rel} . \quad (15)$$

On each side of the cranium, the total stiffness of the muscle spring and connective tissue spring arranged in series is equal to the reciprocal of the sum of the compliances. The total stiffness (k_t) is equal to twice this value (Eqn 9) because the springs on each side of the cranium are arranged in parallel. Substituting the experimentally derived expressions for k_m (Eqn 11) and k_e (mean=1300 N m^{-1}) gives:

$$k_t = 2[(2.303 x_m/c_2 + 1/1300)^{-1}] . \quad (16)$$

The model was implemented for each trial (N=71) from each individual toad (N=4) by: (1) estimating the *in vivo* inertial load ($F_{after}=m_{eff}\boldsymbol{g}$) from anatomical measurements; (2) estimating the total displacement (x_t) from digital images; (3) solving for the unique value of F_{before} that corresponds to the observed total displacement (x_t); and (4) using the value of F_{before} and the equations to calculate x_m, x_e, k_m and k_e.

In the model, connective tissue strain increases linearly with force, whereas muscle strain increases slightly non-linearly with

Table 5. *Elastic properties of the toad cranium predicted from the elastic recoil model in simulations representing the maximum and minimum strain observed for each individual*

Individual	x_m (mm) Max/Min	x_e (mm) Max/Min	k_t (N m^{-1}) Max/Min	b_{eff} (Ns m^{-1}) Max/Min
1	2.2/1.5	1.5/1.0	561/553	4.91/4.88
2	1.8/1.4	1.3/1.0	576/558	4.36/4.28
3	1.3/0.7	1.2/0.7	714/585	4.80/4.35
4	2.0/1.6	1.6/1.3	581/574	4.70/4.67
Mean	1.8/1.3	1.4/1.0	608/567	4.69/4.54
s.e.m.	0.2/0.2	0.09/0.1	36/7	0.12/0.14

x_m, muscle strain; x_e, connective tissue strain; k_t, total spring constant; b_{eff}, effective damping coefficient.

force (Fig. 12A). At all but the lowest forces (<0.25 N), strain in the depressor mandibulae muscles is greater than strain in the extra-muscular connective tissues. Estimated maximum depressor mandibulae strain *in vivo* ranged from 1.3 to 2.2 mm, and estimated maximum connective tissue strain *in vivo* ranged from 1.2 to 1.6 mm (Table 5). In the *in situ* experiments (load-clamp and series connective tissue strain), the force that develops in the depressor mandibulae muscles (i.e. maximum isometric force) is higher than that achieved *in vivo* (i.e. voluntary force). Thus, the estimated *in vivo* displacement of the depressor mandibulae muscles and extra-muscular connective tissues is smaller than that observed *in situ*, as expected.

In the model, the total stiffness (k_t) during elastic recoil varies non-linearly as a function of both the force that develops prior to movement and the external load during movement (Fig. 12B). During elastic recoil, the total stiffness is greater either when the force before movement is smaller or when the external load is larger (i.e. whenever ΔF is smaller). The elastic properties of muscle during elastic recoil thus differ substantially from the elastic properties of both inactive muscle, in which stiffness increases non-linearly with stretch, and active muscle under isometric conditions, in which stiffness increases linearly with force.

The model contains three sources of random error, including the confidence intervals for the slopes of the coefficients c_1 and c_2 with respect to total force (Fig. 9C) and variation among individuals in the stiffness of the extra-muscular connective tissues (Fig. 10B). Because these sources of error are statistically independent, the probability that all three variables will exhibit values outside their 95% confidence intervals simultaneously is equal to $(0.05)^3$, or 0.000125. Thus, the 95% confidence interval for the model as a whole was calculated from the 62.8% confidence intervals for each of the three variables [$1–(0.628)^3=0.05$; Fig. 12C, dotted lines]. The 95% confidence intervals of the model as a whole are relatively large because the estimated values of each variable are based upon relatively small samples (N=3–6).

The elastic recoil model was tested by comparing the total spring constant (k_t) estimated from *in vivo* kinematics using Eqn 3 (Table 1) to the values of k_t predicted by the elastic recoil model (Table 5). In general, there is a good match between the observed and predicted parameters (Fig. 12C). The observed values of k_t ranged from 508–712 N m^{-1}, with a mean of 581±47 N m^{-1} (Table 1). Values of k_t predicted by the model ranged from 550 to 714 N m^{-1}, with a mean of 608±37 N m^{-1} (Table 5). For all four individuals, the values of k_t estimated from kinematics were well within the 95% confidence interval for the k_t predicted by the elastic recoil model and *vice versa* (Fig. 12C).

Discussion

Ballistic mouth opening during feeding in toads

In vivo studies of ballistic mouth opening in toads suggest that elastic strain energy is stored during activation of the depressor mandibulae muscles prior to mouth opening, and that strain energy is recovered during ballistic mouth opening. During ballistic prey capture, the jaws of toads open to angles of up to 60° in less than 20 ms. The depressor mandibulae muscles and series connective tissues shorten by up 21.4% of the muscle's resting length. The muscle mass-specific peak instantaneous power output of the depressor mandibulae muscles and associated connective tissues is up to 9600 W kg^{-1}, more than 25 times the power output of frog hip extensors (m. semimembranosus) during jumping (Lutz and Rome, 1994). The high instantaneous velocities, accelerations and power output support the hypothesis that the mechanism of ballistic mouth opening involves the storage and recovery of elastic strain energy.

Electromyograms synchronized with digital images of freely behaving toads demonstrate that the depressor mandibulae muscles are active for up to 250 ms prior to the onset of ballistic mouth opening. The depressor mandibulae muscles are deactivating, or electrically silent, during ballistic mouth opening (Fig. 6). It appears that de-activation during movement may increase the efficiency of recovery of elastic strain energy. Lou et al. showed (Lou et al., 1999) that work stored in the series elastic component of dogfish axial muscle could be recovered completely as external work when the muscle shortened during relaxation, whereas only 80% of the work was recovered if the muscle remained active during shortening.

Strain of elastic elements in series with the depressor mandibulae muscles

Digital imaging demonstrates that both the cranium, at the muscle's origin, and the retroarticular process, at the muscle's insertion, are strained during *in situ* stimulation of the depressor mandibulae muscles. The average total strain in extra-muscular connective tissues (at the origin and insertion combined) resulting from depressor mandibulae stimulation increases linearly with muscle force, and reaches strains of up to 14% *ML* at maximum isometric force. The measured strain is higher than expected, especially given the short length (<1 mm) of the aponeurosis (i.e. broad, flat tendon) that connects the depressor mandibulae muscle to the retroarticular process of the lower jaw. Most of the strain (12% *ML*) is borne by the retroarticular process itself along the line of action of the depressor mandibulae muscles. Although the observed strain in extra-muscular connective tissues is relatively large, it is not sufficient to account for the maximum total strain observed *in vivo* (i.e. up to 21.4% *ML* at *in vivo* forces estimated to be <70% of maximum isometric force). Thus, sources of strain in addition to the extra-muscular connective tissues must necessarily contribute to the total strain observed *in vivo*.

Strain within the depressor mandibulae muscles

In situ load-clamp experiments were used to quantify the elastic properties of the depressor mandibulae muscles themselves. During rapid unloading, the depressor mandibulae muscles behave as non-linear springs. The elastic properties of

the muscle are determined by: (1) the force achieved prior to movement, and (2) the change in force during unloading. For a given level of muscle force, the displacement from equilibrium increases exponentially as the change in force increases (Eqn 10, Fig. 9A). The spring constant (k_m) decreases non-linearly with the change in force (ΔF), a function of both the force that develops before movement and the external load during movement (Fig. 9B).

Load-clamp experiments demonstrate that the depressor mandibulae muscles of toads experience large displacements from equilibrium when the change in force is large. Depressor mandibulae muscles of 16.3–17 mm resting length were observed to shorten by up to 2.5–3.0 mm (15.3–17.5% *ML*) when the load was decreased rapidly following 200 ms of supramaximal stimulation. The corresponding changes in force were 2.45–3.34 N (2.48–3.42 N before the load-clamp minus 0.03–0.08 N during the load-clamp). In preliminary studies, we also have observed large strains at low loads during *in situ* load-clamp experiments in other anuran muscles. For example, strains of up to 16% *ML* are observed in the semimembranosus muscles of *Rana pipiens* using similar techniques (Pilarski et al., 2003). Previous studies typically report strains of 2–6% in the series elastic component of active muscle (Jewell and Wilkie, 1958; Akimoto and Sugi, 1999; Lou et al., 1999).

Accounting for the observed strain during load-clamp experiments

In the load-clamp preparation, many sources contribute to the total observed strain. Sources external to the depressor mandibulae muscles include: (1) the microfilament connection between muscle and lever, and (2) the cranium at the muscle's origin. In the load-clamp experiments, muscle stimulation cannot deform the retroarticular process as it does *in vivo* because the muscle insertion is tied off with microfilament. In load-clamp tests on the microfilament alone, the mean strain was 0.06 mm (0.36% *ML*) and was independent of load over a range of loads that exceeded the maximum isometric force of the muscles used in this study. At maximum isometric force, the strain at the cranial origin of the depressor mandibulae was 2% *ML* during *in situ* supramaximal muscle stimulation (0.34 mm in a 17 mm muscle). Thus, of the 3.0 mm of strain (maximum) that was observed in the depressor mandibulae muscle in load-clamp experiments, only 0.4 mm (13.3%) can be attributed to sources outside the muscle.

In theory, sources of strain within the depressor mandibulae muscle include: (1) parallel elastic elements, which are strained when the muscle is passively stretched to its *in vivo* resting length at the beginning of each load-clamp trial; and (2) series elastic elements within the muscle, including the cross bridges and filament lattice (Huxley and Simmons, 1971; Wakabayashi et al., 1994), which are strained by the shortening of sarcomeres in active muscle. The strain in parallel elastic elements within the depressor mandibulae muscle contributes up to 0.7 mm (23.3%) to the maximum observed strain (3.0 mm). Based on values from the literature, the strain in the cross bridges and sarcomere lattice is ~6 nm per half sarcomere (Huxley, 1974), with 30–50% of the strain in the cross bridges themselves and 50–70% of the strain in the thick and thin filaments (Kojima et al., 1994; Wakabayashi et al., 1994). In a depressor mandibulae sarcomere (1.5 μm), this corresponds to a strain of only 0.14 mm in a 17 mm muscle. The measured strain in parallel elastic elements and the sarcomere lattice accounts for only 0.84 mm (32.3%) of the total 2.6 mm of strain that develops within a 17 mm depressor mandibulae muscle. The source of the additional 1.76 mm of strain (67.7% of the total, or 77 nm per half sarcomere in a 1.5 μm sarcomere) remains to be determined.

Previous studies of strain in the series elastic component of active muscles typically report values of 2–6% *ML* at maximum isometric force. Working with frog sartorius muscle at L_0, and controlling for the total compliance in their apparatus, Jewell and Wilkie reported (Jewell and Wilkie, 1958) that the contribution of the series elastic component to muscle shortening was only 2% of total muscle length at 2°C using clamp loads as low as 3% of P_0. Lou et al. estimated that the series elastic component of red muscle fibers of the dogfish extends by 5% at maximum isometric force and a temperature of 12°C (Lou et al., 2002). Akimoto and Sugi estimated the extension of the series elastic component of horseshoe crab telson muscle at 6% of the slack muscle fiber length at 18–24°C (Akimoto and Sugi, 1999). In horseshoe crab telson, although the relative strain in the series elastic component of muscle fibers is only 6% of the slack sarcomere length, the absolute strain is 210 nm per half sarcomere due to the extreme length of the sarcomeres (7 μm). On the basis of cinematographic studies of isometrically contracting fiber bundles, Sugi et al. suggest (Sugi et al., 2000) that the elastic titin protein, which extends from the M-line to the Z-disk, might contribute to the series elasticity of horseshoe crab telson muscle.

Adaptations of the depressor mandibulae for storage and recovery of elastic strain energy

The depressor mandibulae muscles of toads possess characteristics that suggest that they may be specialized for powering ballistic prey capture. Relative to anuran species that lack ballistic tongue projection, the depressor mandibulae muscles of toads are hypertrophied. Their mass exceeds that of all six pairs of jaw adductor muscles combined, and their physiological cross-sectional area is more than twice that of the largest jaw adductors, the mm. levator mandibulae posterior longus. This hypertrophied condition, relative to the size of the feeding apparatus as a whole, likely enhances the amount of elastic strain energy that can be stored and subsequently recovered to power ballistic prey capture. In addition, the sarcomeres of the depressor mandibulae muscle in toads are shorter (1.5 μm) than is typical for vertebrate striated muscle (e.g. 1.98–2.64 μm) (Burkholder and Lieber, 2001). The shorter length of the sarcomeres is expected to result in greater muscle shortening velocity at the expense of decreased force, relative to typical vertebrate sarcomeres, assuming that the intrinsic rate of sarcomere shortening

remains the same (Eckert, 1988). Therefore, it is somewhat surprising that the V_{max} of toad depressor mandibulae muscles (up to 63.9 mm s^{-1}, or 3.7 *ML* s^{-1}) is both absolutely and relatively much lower than the V_{max} of anuran limb muscles (e.g. semimembranosus of *Rana pipiens*, V_{max}=12 *ML* s^{-1}) (Lutz and Rome, 1994; Lutz and Rome, 1996). Finally, passive tension develops at relatively short sarcomere lengths (97% L_0) in the depressor mandibulae muscles of toads. This may indicate that they possess a relatively short and stiff isoform of titin (see Wang et al., 1991), which would increase both the total elastic energy stored and the rate of recovery of elastic strain energy during ballistic movement.

Elastic recoil model of ballistic mouth opening in toads

In situ measurements of the elastic properties of extra-muscular connective tissues of the cranium and mandible, as well as the depressor mandibulae muscles themselves, were combined to produce an elastic recoil model of ballistic mouth opening during feeding in toads. For a given level of force prior to movement, the model predicts the total displacement (Fig. 12A) and the total stiffness (Fig. 12B,C) during elastic recoil based on the measured elastic properties of the individual components. A major result that emerges from the model is that, over the physiological range of forces for the muscles used in this study, strain is greater in the depressor mandibulae muscles than in the extra-muscular connective tissues, except at the lowest forces (<0.25 N), at which the strains are approximately equal (Fig. 12A).

Due to the non-linear relationships among total displacement, total stiffness and force (Fig. 12A,B, Eqn 15, 16), the elastic recoil model predicts that the total elastic energy stored prior to movement will increase linearly with the force developed by the depressor mandibulae muscles prior to movement. Over the physiological range of muscle forces and *in vivo* loads, the elastic strain energy ($0.5kx^2$) stored in extra-muscular connective tissues is greater than that stored in the depressor mandibulae muscles, due to their greater stiffness (Table 5). The energy stored in these structures is difficult to estimate because the total energy stored in cranial structures prior to movement ($0.5k_tx_t^2$) is less than the sum of the energy that would be stored in the individual components in isolation ($0.5k_ex_e^2+0.5k_mx_m^2$). The reason for the inequality is that the total stiffness of springs arranged in series is equal to the reciprocal of the sum of the compliances, rather than the sum of the spring constants. Theoretically, in isolation, given the respective mean displacements and spring constants of the muscles and extra-muscular connective tissues (Table 5), each muscle spring would store 0.98 mJ of elastic potential energy prior to movement, whereas the extra-muscular connective tissues on each side of the cranium would store 1.27 mJ. The actual estimated energy stored in all spring elements of the toad cranium and mandibles arranged in series is 4.24 mJ, which corresponds well with estimates based on the positive integral of instantaneous power derived from kinematic analyses (Fig. 5B).

Although the energy recovered during movement cannot be greater than the potential energy stored prior to movement, the rate of energy recovery (or power output) depends more strongly on the natural frequency [SQRT(k/m)] than on the elastic potential energy. Therefore, to understand how the recovery of elastic potential energy contributes to the power of ballistic movements, it is important not only to investigate the energy stored prior to movement, but also elastic properties during movement. Historically, analyses of ballistic movements such as jumping have used the equations of projectile motion to estimate the amount and rate of energy recovered during movement, and have measured the contribution of extra-muscular series elastic elements (e.g. tendons) to elastic energy storage prior to movement (e.g. Alexander and Bennet-Clark, 1977). Typically, these studies ignore the relationship between natural frequency and power output, and assume that muscle itself contributes nothing in terms of strain, stiffness, or energy to elastic recoil. However, a complete explanation of ballistic motion requires not only an accounting of whether sufficient energy is stored in extra-muscular springs, but also how elastic properties (i.e. strain and stiffness) contribute to elastic energy storage and the rate of energy recovery.

A classic, well-studied example of the role of elastic strain energy storage and recovery in powering ballistic movements is jumping and kicking in locusts (Bennet-Clark, 1975; Burrows and Morris, 2001). Based on analyses of ballistic motion combined with a detailed analysis of the elastic properties of the cuticle (i.e. semilunar process) and apodeme of the extensor tibiae muscle in locusts whose femora and tibiae ranged in length from 24–25 mm, Bennet-Clark concluded (Bennet-Clark, 1975) that the strain energy stored in these structures is greater than the energy recovered from them during the ballistic movement. However, it is informative to ask whether the strain observed in the cuticle (semilunar process) and apodeme of the extensor tibiae muscle of the locust hindlimb can account for the joint extensions observed during kicking and jumping in locusts, and, if not, how much strain the muscle itself might contribute. A kicking locust extends its leg from 30° to 180° in as little as 3 ms (Burrows and Morris, 2001). Using the law of cosines, if a 25 mm tibia is rotated through an angle of 150° during leg extension, then the displacement of the distal end of the tibia is 48.3 mm. The in-lever/out-lever ratio of the extensor tibiae muscle is 1:35, so the total displacement of the muscle-apodeme-semilunar process complex is 1.4 mm. Bennet-Clark observed (Bennet-Clark, 1975) a maximum strain in the semilunar process of 0.4 mm and in the extensor tibiae muscle apodeme of 0.48 mm, together accounting for only 63% (0.88/1.4 mm) of the total strain necessary for leg extension in a locust with a 25 mm tibia. If the extensor tibiae muscle were to provide this additional strain, it would need to shorten by 0.52 mm (12% of the length of its longest fibers) at a rate of 40 *ML* s^{-1}. These values are within the range of strains (Tables 1, 5) and strain rates (Table 2) observed in the depressor mandibulae muscles of toads in the present study.

Implication for CNS control of ballistic mouth opening

Despite its relatively simple anatomical arrangement, the ballistic tongue projection system of toads exhibits a variety of interesting properties, including modulation based on distance to target as well as dynamic stability under perturbations in external load. Our results demonstrate that an elastic recoil model performs well at predicting the energy storage, displacement, velocity and power output of ballistic mouth opening. This implies that the central nervous control of ballistic mouth opening in toads might be relatively simple in principle. The time-dependent behavior of a mass–spring system during elastic recoil from rest is governed by four variables: mass, displacement, stiffness and damping coefficient. All four variables scale predictably with body size, so that the elastic recoil model can be used to predict how ballistic movements should differ among individuals of different sizes (K. C. Nishikawa, A. K. Lappin, C. P. McGowan and J. C. O'Reilly, manuscript in preparation). Within individuals, both the effective mass (i.e. external load during movement) and the damping coefficient (just below critical damping) are relatively constant from trial to trial, whereas total displacement and total stiffness vary up to twofold from trial to trial within individuals (Table 1), depending at least in part on the distance to prey.

Because the stiffness of the extra-muscular connective tissues is constant, the load-dependence of the elastic properties of the toad's mass–spring system arise from the behavior of the depressor mandibulae muscles during elastic recoil. Load-clamp experiments demonstrate that both the displacement and stiffness of the depressor mandibulae muscles depend on the change in force (ΔF) during rapid unloading. The change in force itself depends upon the force that develops in the depressor mandibulae muscles prior to movement, as well as the external load during movement. Because the external load is relatively constant from trial to trial, the elastic properties of the toad's ballistic mouth-opening system are determined in large part by the force that develops in the depressor mandibulae muscles prior to movement. However, if the load changes unexpectedly, the total stiffness will adjust automatically without requiring neural input. The system will become stiffer if the external load increases, and will become less stiff if the load decreases (Fig. 12B).

Mallett et al. showed that ballistic tongue projection is dynamically stable, and that more than 90% of the force of tongue projection comes from transfer of momentum from the opening jaws to the tongue (Mallett et al., 2001). In principle, it appears that the central nervous system could control ballistic mouth opening in toads by specifying only the initial force in the jaw muscles and the timing of rapid unloading. The resulting movement of the jaws and tongue is determined by the load-dependent elastic properties of the ballistic mouth-opening system.

Recent studies have demonstrated that intrinsic musculoskeletal properties, such as the force–length and force–velocity behavior of muscle, can stabilize movement and simplify control (Brown and Loeb, 2000; Jindrich and Full, 2002; Aoyagi et al., 2004; Richardson et al., 2005). For ballistic movements, the after-loaded force–velocity behavior is largely irrelevant, whereas the non-linear, load-dependent stiffness of muscle during elastic recoil simplifies control and also provides stability during unexpected perturbations in load.

List of symbols

ζ	damping ratio
ω_d	damped frequency of vibration
ω_n	natural frequency of vibration
a	acceleration
b_{eff}	effective damping coefficient
F_{rel}	relative force (P/P_0)
F_t	total force
$\boldsymbol{g}$	gravitational constant
k_e	spring constant of the extra-muscular connective tissues
k_m	spring constants of the depressor mandibulae muscles
k_t	total spring constant
L_0	optimum length of greatest active force production
l_m	muscle length
m_{eff}	total effective mass
ML	muscle length
P	force
P_0	maximum isometric force
t	time
v	instantaneous velocity
v_0	initial velocity
V	velocity
V_{max}	maximum shortening velocity
x_e	connective tissue spring displacement
x_m	muscle spring displacement
x_t	total displacement
x_0	initial displacement

We thank R. McNeill Alexander for inspiring these inquiries into elastic energy storage and recovery during ballistic tongue projection. Tom Daniel provided invaluable help with model development and implementation, as well as logistical support during the preparation of this manuscript. Bertram Tanner and Michael Tu helped with the development of Matlab programs for calculating time integrals and fitting the Hill equation. Tom Daniel, Stephen Deban, Tyson Hedrick, Steve Hempleman, Stan Lindstedt, Sanjay Sane and Steve Warburton provided numerous helpful suggestions on the design, analysis, and interpretation of our experiments, as well as insightful comments for improving the manuscript. This research was supported by grants IBN-0215438 and IBN-0240349 from the National Science Foundation, and R25-GM56931 from the National Institutes of Health.

References

Aerts, P. (1998). Vertical jumping in *Galago senegalensis*: the quest for an obligate mechanical power amplifier. *Philos. Trans. R. Soc. Lond. B Biol. Sci.* **353**, 1607-1620.

Akimoto, T. and Sugi, H. (1999). Origin of the series elastic component in horseshoe crab skeletal muscle fibers. *Comp. Biochem. Physiol.* **122A**, 139-144.

Alexander, R. McN. (1968). *Animal Mechanics*. Seattle: University of Washington Press.

Alexander, R. McN. (1988). *Elastic Mechanisms in Animal Movement*. Cambridge: Cambridge University Press.

Alexander, R. McN. (2002). Tendon elasticity and muscle function. *Comp. Biochem. Physiol.* **133A**, 1001-1011.

Alexander, R. M. and Bennet-Clark, H. C. (1977). Storage of elastic strain energy in muscle and other tissues. *Nature* **265**, 114-117.

Aoyagi, Y., Stein, R. B., Mushawar, V. K. and Prochazka, A. (2004). The role of neuromuscular properties in determining the end-point of a movement. *IEEE Trans. Neural Syst. Rehab. Eng.* **12**, 12-23.

Askew, G. N. and Marsh, R. L. (1998). Optimal shortening velocity (V/V_{max}) of skeletal muscle during cyclical contractions: length–force effects and velocity-dependent activation and deactivation. *J. Exp. Biol.* **201**, 1527-1540.

Bennet-Clark, H. C. (1975). Energetics of the jump of the locust *Schistocerca gregaria*. *J. Exp. Biol.* **63**, 53-83.

Brown, I. E. and Loeb, G. E. (2000). A reductionist approach to creating and using neuromusculoskeletal models. In *Biomechanics and Neural Control of Posture and Movement* (ed. J. M. Winters and P. E. Crago), pp. 148-163. New York: Springer-Verlag.

Burkholder, T. J. and Lieber, R. L. (2001). Sarcomere length operating range of vertebrate muscles during movement. *J. Exp. Biol.* **204**, 1529-1536.

Burrows, M. and Morris, G. (2001). The kinematics and neural control of high-speed kicking movements in the locust. *J. Exp. Biol.* **204**, 3471-3481.

Deban, S. M. and Dicke, U. (1999). Motor control of tongue movement during prey capture in plethodontid salamanders. *J. Exp. Biol.* **202**, 3699-3714.

Deban, S. M., Wake, D. B. and Roth, G. (1997). Salamander with a ballistic tongue. *Nature* **389**, 27-28.

de Groot, J. H. and van Leeuwen, J. L. (2004). Evidence for an elastic projection mechanism in the chameleon tongue. *Proc. R. Soc. Lond. B Biol. Sci.* **271**, 761-770.

Eckert, R. D. (1988). *Animal Physiology: Mechanisms and Adaptations* (3rd edn). New York: W. H. Freeman.

Ford, L. E., Huxley, A. F. and Simmons, R. M. (1977). Tension responses to sudden length change in stimulated frog muscle fibres near slack length. *J. Physiol.* **269**, 441-515.

Hill, A. V. (1938). The heat of shortening and the dynamic constants of muscle. *Proc. R. Soc. Lond. B Biol. Sci.* **126**, 136-195.

Huxley, A. F. (1974). Muscular contraction. *J. Physiol.* **243**, 1-43.

Huxley, A. F. and Simmons, R. M. (1971). Proposed mechanism of force generation in striated muscle. *Nature* **233**, 533-538.

Jewell, B. R. and Wilkie, D. R. (1958). An analysis of the mechanical components in frog's striated muscle. *J. Physiol.* **143**, 515-540.

Jindrich, D. L. and Full, R. J. (2002). Dynamic stabilization of rapid hexapedal locomotion. *J. Exp. Biol.* **205**, 2803-2823.

Kojima, H., Ishijima, A. and Yanagida, T. (1994). Direct measurement of stiffness of single actin filaments with and without tropomyosin by in vitro nanomanipulation. *Proc. Natl. Acad. Sci. USA* **91**, 12962-12966.

Lou, F., Curtin, N. A. and Woledge, R. C. (1999). Elastic energy storage and release in white muscle from dogfish *Scyliorhinus canicula*. *J. Exp. Biol.* **202**, 135-142.

Lou, F., Curtin, N. A. and Woledge, R. C. (2002). Isometric and isovelocity contractile performance of red muscle fibres from the dogfish *Scyliorhinus canicula*. *J. Exp. Biol.* **205**, 1585-1595.

Lutz, G. J. and Rome, L. C. (1994). Built for jumping: the design of the frog muscular system. *Science* **263**, 370-372.

Lutz, G. J. and Rome, L. C. (1996). Muscle function during jumping in frogs. II. Mechanical properties of muscle: implications for system design. *Am. J. Physiol.* **271**, C571-C578.

Mallett, E. S., Yamaguchi, G., Birch, J. M. and Nishikawa, K. C. (2001). Feeding motor patterns in anurans: insights from biomechanical modeling. *Am. Zool.* **41**, 1364-1374.

Meyers, J. J. and Nishikawa, K. C. (2000). Mechanisms of tongue protrusion in iguanian lizards, with comments on tongue projection in chameleons. *J. Exp. Biol.* **203**, 2833-2849.

Monroy, J. A. and Nishikawa, K. C. (2003). Modulation of muscle pre-activation as a function of prey distance in freely behaving toads. *Int. Comp. Biol.* **42**, 1281.

Nishikawa, K. C. (1999). Neuromuscular control of prey capture in frogs. *Philos. Trans. R. Soc. Lond. B Biol. Sci.* **354**, 941-954.

Nishikawa, K. C. (2000). Feeding in frogs. In *Feeding, Form, Function, and Evolution in Tetrapod Vertebrates* (ed. K. Schwenk), pp. 117-147. San Diego: Academic Press.

Nishikawa, K. C. and Gans, C. (1992). The role of hypoglossal sensory feedback during feeding in the marine toad, *Bufo marinus*. *J. Exp. Zool.* **264**, 245-252.

Nishikawa, K. C. and Gans, C. (1996). Mechanisms of prey capture and narial closure in the marine toad, *Bufo marinus*. *J. Exp. Biol.* **199**, 2511-2529.

Nishikawa, K. C., Kier, W. M. and Smith, K. K. (1999). Morphology and mechanics of tongue movement in the African pig-nosed frog *Hemisus marmoratum*: a muscular hydrostatic model. *J. Exp. Biol.* **202**, 771-780.

Peplowski, M. M. and Marsh, R. L. (1997). Work and power output in the hind limb muscles of Cuban tree frogs, *Osteopilus septentrionalis* during jumping. *J. Exp. Biol.* **200**, 2861-2870.

Pilarski, J. Q., Philips, G., Nishikawa, K. C. and Pierotti, D. J. (2003). Power amplification by pre-activation of hind limb muscle during jumping in frogs. *FASEB J.* **17**, A1287.

Richardson, A. G., Slotine, J. J., Bizzi, E. and Tresch, M. C. (2005). Intrinsic musculoskeletal properties stabilize wiping movements in the spinalized frog. *J. Neurosci.* **25**, 3181-3191.

Sugi, H., Akimoto, T., Kobayashi, T., Suzuki, S. and Shimada, S. (2000). Possible contribution of titin filaments to the compliant series elastic component in horseshoe crab skeletal muscle fibers. *Adv. Exp. Med. Biol.* **481**, 371-380.

Wainwright, P. C. and Bennett, A. F. (1992a). The mechanism of tongue projection in chameleons. I. Electromyographic tests of functional hypotheses. *J. Exp. Biol.* **168**, 1-21.

Wainwright, P. C. and Bennett, A. F. (1992b). The mechanism of tongue projection in chameleons. II. Role of shape change in a muscular hydrostat. *J. Exp. Biol.* **168**, 23-40.

Wakabayashi, K., Sugimoto, Y., Tanaka, H., Ueno, Y., Takezawa, Y. and Amemiya, Y. (1994). X-ray evidence for the extensibility of actin and myosin filaments during muscle contraction. *Biophys. J.* **67**, 2422-2435.

Walker, J. A. (1998). Estimating velocities and accelerations of animal locomotion: a simulation experiment comparing numerical differentiation algorithms. *J. Exp. Biol.* **201**, 981-995.

Wang, K., McCarter, R., Wright, J., Beverly, J. and Ramirez-Mitchell, R. (1991). Regulation of skeletal muscle stiffness and elasticity by titin isoforms: a test of the segmental extension model of resting tension. *Proc. Natl. Acad. Sci. USA* **88**, 7101-7105.